



# Effect of crustal stress state on magmatic stalling and ascent: case study from Puyehue-Cordón Caulle, Chile

Katy J. Chamberlain<sup>1,2</sup> · Daniel J. Morgan<sup>3</sup> · Luis E. Lara<sup>4,5</sup> · Richard Walshaw<sup>3</sup> · Joe Gardner<sup>2</sup> · Simon Chenery<sup>6</sup> · Ian L. Millar<sup>6</sup> · Doris Wagner<sup>6</sup>

Received: 8 October 2023 / Accepted: 15 April 2024  
© The Author(s) 2024

## Abstract

The Southern Volcanic Zone (SVZ) in Chile is an active continental arc with a complex history of volcanism, where a range of magmatic compositions have been erupted in a variety of styles. In the Central SVZ, both monogenetic and polygenetic volcanoes exist, in close proximity to the Liquiñe-Ofqui Fault System (LOFS), but with variable local stress states. Previous studies have inferred varying crustal storage timescales, controlled by the orientation of volcanic centres relative to the N-S striking LOFS and  $\sigma_{\text{HMax}}$  in this region. To assess the relationship between volcanism and crustal stress states affected by large-scale tectonic structures and edifice controls, we present whole rock geochemical data, to ensure consistency in source dynamics and crustal processing, mineral-specific compositional data, thermobarometry, and Fe–Mg diffusion modelling in olivine crystals from mafic lavas, to assess ascent timescales, from the stratovolcanic edifice of Puyehue-Cordón Caulle and proximal small eruptive centres. Textural observations highlight differences in crystal maturation timescales between centres in inferred compression, transpression, and extension, yet source melting dynamics remain constant. Only samples from the stratovolcanic edifice (in regional compression) preserve extensive zonation in olivine macrocrysts; these textures are generally absent from proximal small eruptive centres in transtension or extension. The zonation in olivines from stratovolcanic lavas yields timescales on the order of a few days to a few weeks, suggesting that even in environments which inhibit ascent, timescales between unrest and eruption of mafic magmas may be short. Significantly, high-resolution compositional profiles from olivine grains in the studied samples record evidence for post-eruptive growth and diffusion, highlighting the importance of careful interpretation of diffusion timescales from zoned minerals in more slowly cooled lavas when compared with tephra samples.

**Keywords** Diffusion chronometry · Arc volcanism · Magma ascent

---

Editorial responsibility: J.E. Hammer

✉ Katy J. Chamberlain  
k.j.chamberlain@liverpool.ac.uk

- <sup>1</sup> Environmental Sustainability Research Centre, University of Derby, Derby, UK
- <sup>2</sup> Department of Earth, Ocean & Ecological Sciences, University of Liverpool, Liverpool, UK
- <sup>3</sup> Institute of Geophysics and Tectonics, School of Earth & Environment, University of Leeds, Leeds, UK
- <sup>4</sup> Instituto de Ciencias de La Tierra, Universidad Austral de Chile, Valdivia, Chile
- <sup>5</sup> Instituto Milenio Ckelar Volcanes, Antofagasta, Chile
- <sup>6</sup> Geochronology & Tracers Facility, British Geological Survey, Nottingham, UK

## Introduction

Understanding when, and for how long, volcanic eruptions will occur is a pivotal question in volcanological research, and allows for better hazard management (Sparks 2003; Coombs et al. 2018). Petrological studies allow magmatic processes and timescales to be determined from past eruptions (e.g. Blundy and Cashman (2008), Costa et al. (2020), and Wilson et al. (2021)), which, when integrated with geophysical monitoring of unrest at active volcanoes, can allow more accurate forecasts of timing of volcanic activity (for example, Giuffrida et al. (2021) and Kahl et al. (2022)). However, in order for magma to ascend and eruptions to occur, dyke formation must be favored, and this process is fundamentally controlled by the stress state of the crust (Watanabe et al. 1999; Rivalta et al. 2005;

Kavanagh et al. 2018). Whilst significant advancements have been made in understanding how magmas ascend through the crust in different stress states (e.g. Pinel and Jaupart (2000), Rivalta et al. (2019), and Caricchi et al. (2021)), the link between ascent processes and the duration and amount of pre-eruptive unrest, under different crustal stress conditions, still requires development.

Many methods exist for determining timescales of magmatic processes (see Costa et al. 2020 for review), but diffusion chronometry has become a widely applied tool to understand timescales associated with pre-eruptive magmatic processes, from storage (e.g. Mutch et al. (2019a) and Lubbers et al. (2022)) to mixing (e.g. Chamberlain et al. (2014), Longpre et al. (2014), and Mangler et al. (2022)) and ascent (e.g. Morgado et al. (2019), Mutch et al. (2019a, b), and Couperthwaite et al. (2020)). Diffusion chronometry is a powerful technique to constrain magmatic timescales, applying models of varying complexity to compositional gradients preserved within mineral grains, data for which can be obtained via back-scatter electron (BSE) or cathodoluminescence (CL) images, or measured major (electron probe micro analysis: EPMA) or trace elemental (secondary ion mass spectrometry: SIMS, laser ablation inductively coupled plasma mass spectrometry: LA-ICPMS) abundances. Whilst all diffusion models contain many inbuilt assumptions, and recent work has highlighted the potential for post-eruptive relaxation of composition profiles (e.g. Bell et al. (2023), Conway et al. (2020), and Couperthwaite et al. (2020, 2021)), carefully constrained diffusion chronometry data can help build a more complete picture of magmatic processes.

The Puyehue-Cordón Caulle volcanic complex (PCCVC), in the central Southern Volcanic Zone (SVZ), is an ideal location to study the relationship between timescales of magmatic processes and stress state, because extensive studies have constrained the magma source (e.g. Gerlach et al. (1988), Hickey-Vargas et al. (2002, 2016a, b), and Jicha et al. (2007)), magmatic evolution (e.g. Lara et al. (2006b), Jicha et al. (2007), Singer et al. (2008), and Alloway et al. (2015)), and tectonic and crustal stress states (e.g. Lara et al. (2006a, 2006b) and Cembrano and Lara (2009)) of the region, but there is limited work on quantifying magmatic timescales. Additionally, the Puyehue edifice (located at the intersection of the ca. 1200-km-long Liquiñe-Ofqui Fault System (LOFS) with the Cordón Caulle Fissure, thought to be rooted in a margin transversal fault) has been ascribed to a local compressional domain (Cembrano and Lara 2009). Proximal to the PCCVC stratovolcanic edifices multiple mafic, small eruptive centres (SEC) exist. The SEC have distinct orientations and alignments relative to the regional stress state (Lara et al. 2006b), suggesting that they are either in local extension (e.g. the northern Carrán-Los Venados group (Lara et al. 2006a; Bucchi et al. 2015) and southern Antillanca Volcanic Complex (Naranjo et al. 2017)) or that are

parallel with the regional LOFS structure (Anticura, Lara et al. 2006a).

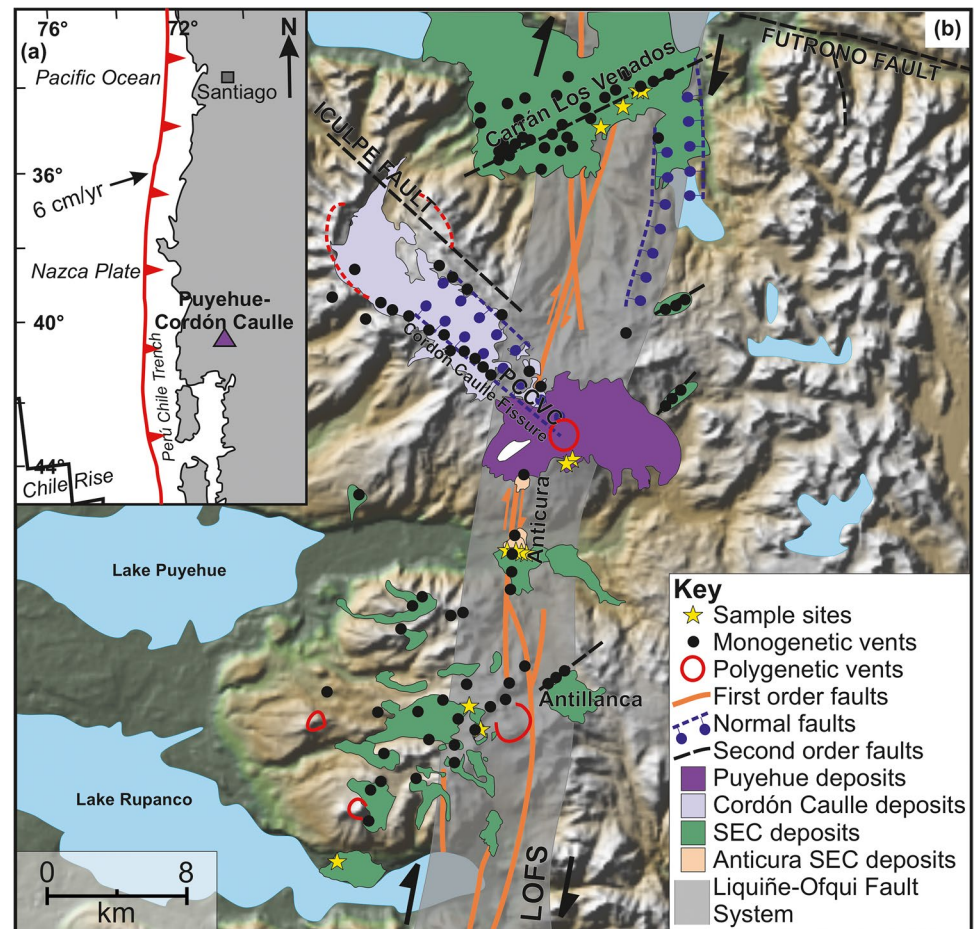
In this study, mafic lavas and spatter samples erupted from vents associated with different inferred stress states from across the PCCVC and surrounding area have been collected. Only mafic samples are considered here to minimise the effects of fractional crystallization, and to limit the number of variables which may affect magmatic ascent (including for example viscosity and magma density). Whole rock major, trace, and isotopic data on these samples are presented to assess the role of different melt source and evolution in the regional area. Then, detailed petrological study and modelled olivine Fe–Mg diffusion timescales from the same samples are combined with pre-existing knowledge of stress states of volcanic edifices in the PCCVC to examine the relationship between magma residence and ascent timescales and local stress conditions (cf. Cembrano & Lara 2009 and Zellmer et al. 2014).

## Geological and structural setting

The Puyehue-Cordón Caulle Volcanic Complex is located in the centre of the SVZ of Chile at 40.5° S, 72.2° W, 85 km east of the city of Osorno. The SVZ is a 1400-km-long active continental arc, with more than fifty arc-front volcanic edifices, of which the PCCVC is one. The SVZ results from the oblique subduction of the Nazca plate under the South American plate at a rate of 6 mm/year (Fig. 1a, Angermann et al. 1999). In the SVZ, the oblique convergence is partitioned into margin-orthogonal compression in the forearc, and right-lateral strike-slip transpression along the arc, in part accommodated along the extensive Liquiñe-Ofqui Fault System (LOFS): a ~1200-km-long dextral strike-slip fault system consisting of multiple NNE striking lineaments (Cembrano et al., 1996). Quaternary volcanoes in the SVZ align along the LOFS, as well as in NW and NE-trending groups oblique to the LOFS (Cembrano & Lara 2009). The continental crust in the southernmost segment is ~35 km thick, and is composed of igneous, metamorphic, and sedimentary lithologies of Oligocene–Miocene age (Singer et al. 2008 and references therein).

The PCCVC is a complex comprising two stratovolcanoes, Puyehue and Cordillera Nevada, the latter partially collapsed, and a fissure system connecting them from which evolved magmas have been erupted during the Holocene (Fig. 1). Puyehue volcano is located at the intersection of the PCCVC and the LOFS. The ~130 km<sup>3</sup> PCCVC consists of Pleistocene to Holocene volcanic rocks, which have been emplaced over a period of ca. 500 kyr (Singer et al. 2008). Early shield volcanic structures have been eroded, and extensive <sup>40</sup>Ar/<sup>39</sup>Ar dating has constrained the oldest exposed products of the Puyehue stratovolcano to an eruption

**Fig. 1** (a) Tectonic setting of Puyehue-Cordón Caulle complex relative to the arc-front and major tectonic features (adapter from Singer et al. (2008)) and (b) location map of the Puyehue-Cordón Caulle Volcanic Complex (PCCVC) with the locations of collected samples highlighted as yellow stars. Known fault traces shown in white, with the Liquiñe-Ofqui Fault System (LOFS) shown as a white zone running roughly N-S. Adapted from Gilbert (2012) and Lara et al. (2006a) and modified from the 1:50,000 scale base map by Lara and Moreno (2006)



at ~69 ka (with the most recent eruptions at ~1.1 ka; Lara et al. 2006b; Singer et al. 2008). Detailed mapping of the Puyehue edifice has shown that the stratocone is composed of both tephra and lavas, of basaltic to rhyolitic compositions (Lara et al. 2006b; Singer et al. 2008). The more evolved fissure system of Cordón Caulle has a modern history of eruption, filling the NW-trending graben (defined by an unnamed northern fault, and the southern Cordón Caulle fissure, Sepúlveda et al. 2005) from 19 ka to present, and was the source of the most recent activity across the entire PCCVC in 1921–1922, 1960, and 2011–2012 CE. These eruptions produced rhyodacite to rhyolitic lavas and tephra (Lara et al. 2004; Singer et al. 2008; Schipper et al. 2013).

Magmas erupted from Puyehue span a continuum from basalt (up to 10 wt.% MgO) to rhyolite (Gerlach et al. 1988; Jicha et al. 2007) with the basalts erupted at PCCVC being some of the most MgO-rich in the SVZ. However, whole rock isotopic work suggests that these basalts have also undergone melting and assimilation of lower crustal material (Jicha et al. 2007). Previous work has shown that the suite of rocks erupted from the PCCVC are connected through extensive, potentially polybaric, fractional crystallization and storage, with minor components of magma mixing

occurring in the lower to middle crust (Gerlach et al. 1988; Jicha et al. 2007; Alloway et al. 2015; Winslow et al. 2022). Generally, uniform  $^{230}\text{Th}/^{232}\text{Th}$  ratios of Puyehue lavas have been used to suggest that the mantle source for magmas at PCCVC is relatively homogenous (Jicha et al. 2007). Isotopic and trace element data from the PCCVC has shown that low-degree fluid-fluxed melting coupled with assimilation of lower crustal materials generated the magmas that feed volcanism, with no evidence for significant differences in slab input or degree of melting between the Puyehue edifice and the Anticura monogenetic cones (Lara et al. 2006a; Jicha et al. 2007).

Whilst the mantle source appears constant between the Puyehue edifice and the Anticura SEC, the upper crustal stress states and inferred crustal magmatic residence time-scales have been suggested to differ by Lara et al. (2006a), and Cembrano and Lara (2009). A similar picture is proposed at regional scales by Pérez-Estay et al. (2023), where diversity is recognised in terms of local stress regime and inferred magma pathways. The PCCVC is an example of basement-controlled—and hence mostly compressional—volcanic complex (Cembrano & Lara 2009), which is rooted on oblique NW-trending structures, pre-Andean

in origin (e.g. Futrono Fault, with a local expression in the Iculpe River Fault, Fig. 1). However, seismic evidence points to a hybrid strike-slip plus extensional regime in this area, which is consistent with the surface morphology. In fact, Cordon Caulle fissure system is parallel to transversal structures (Fig. 1, Lara et al. 2006a) and lies inside a graben structure (Sepúlveda et al. 2005). Thus, the limited structural data combined with volcano morphometry (e.g. edifice and crater alignments) is consistent with the regional view of oblique chains being compressional domains in the long-term, with longer inferred magma residence timescales within the crust (Lavenu & Cembrano 1999; Lara et al. 2004; Cembrano & Lara 2009), although changes in stress state can be recognised during eruptive episodes. NE-trending volcanic edifices and structures are present in the PCCVC region (both north and south

of the stratovolcanic complex), and are inferred to represent extensional domains with their alignment (N65°E) exemplifying the current orientation of the far-field maximum horizontal stress axis (N60°E, Rosenau et al. 2006; Cembrano & Lara 2009; Bucchi et al. 2015). The Carrán-Los Venados volcanic group (Lara et al. 2006a; Bucchi et al. 2015) and southern Antillanca Volcanic Complex (Lara et al. 2006a; Naranjo et al. 2017) are clusters of SEC that align on NE-trending structures (some of which are second-order faults, Fig. 2). Finally, some SEC align N-S along the LOFS, in this region consisting of a series of NNE lineaments. The Anticura SEC are examples of these volcanic centres aligned N-S along the LOFS, with inferred intermediate crustal residence timescales between other centres in compression (PCCVC) and centres in extension (CLV, Antillanca, Lara et al. 2006a).

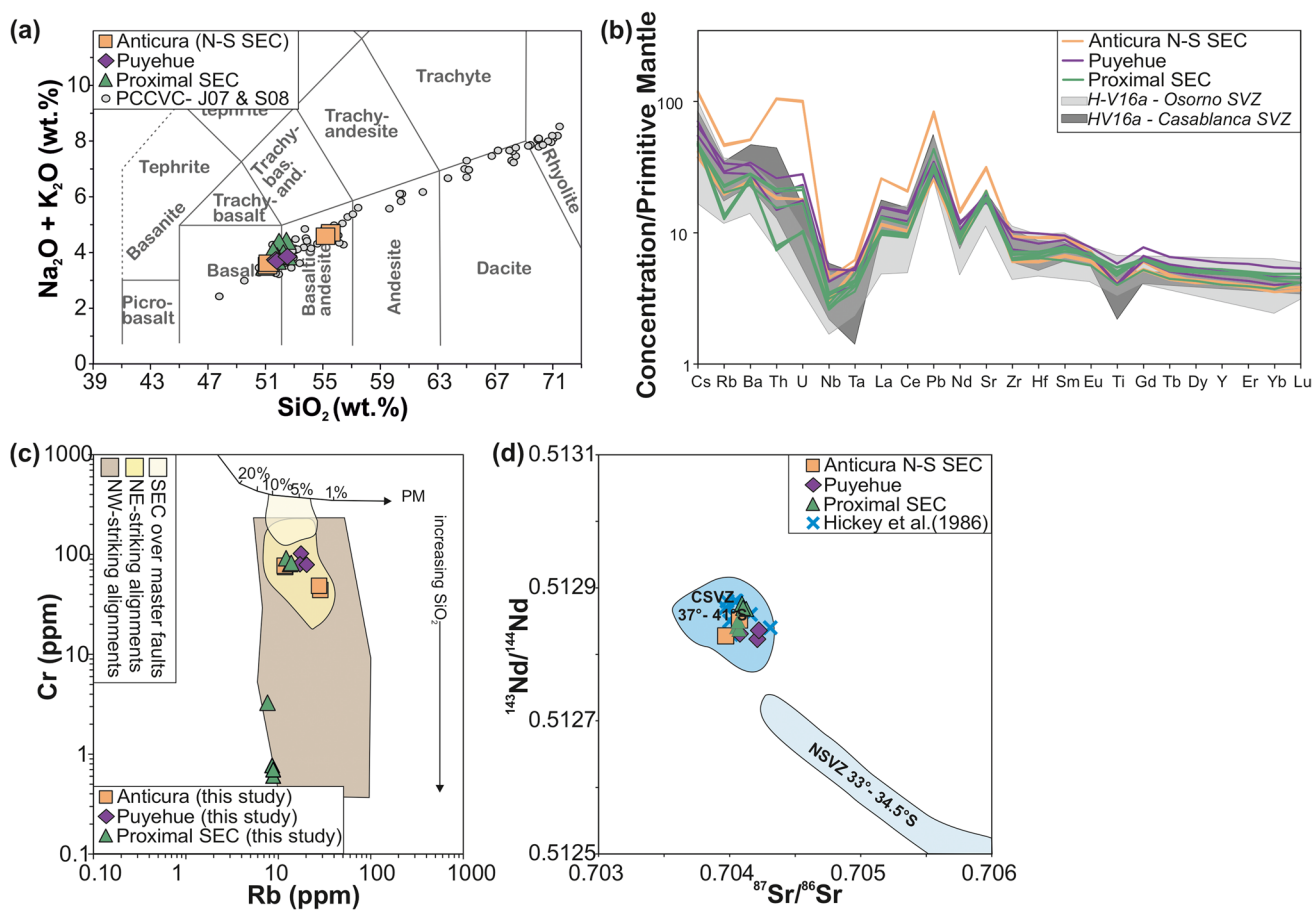


**Fig. 2** Whole rock data summary from this study (orange squares, purple diamonds and green triangles) and selected other studies (see individual legends). Uncertainty on values is smaller than the size of points on scatter graphs. (a) Total alkali-silica plot after Le Maitre (1984). Whole rock data from the entire Puyehue-Cordon Caulle Volcanic Complex from Jicha et al. (2007) [J07] and Singer et al. (2008) [S08]; (b) primitive mantle normalised (Sun & McDonough 1989) trace element spider plot from this work with two fields from

Volcan Osorno and Volcan Casablanca stratovolcanic centres within 70 km or PCCVC in the SSVZ, from Hickey-Vargas et al. (2016a); (c) Rb vs. Cr for samples of this study compared with the southern SVZ classifications after Cembrano and Lara (2009); (d) radiogenic Sr and Nd isotope plot after Hickey et al. (1986) with fields for the central Southern Volcanic Zone (CSVZ) and northern Southern Volcanic Zone (NSVZ) shown in blue. Our data as filled symbols, data from Hickey et al. (1986) as blue crosses

## Methods

### Sampling and whole rock geochemistry

Samples of (rapidly cooled) rumbly tops of mafic lavas and spatter cones were collected from the monogenetic Anticura cones (< 5.9 ka, Lara et al. 2006a; Fig. 1), and the young (~ 43 ka [Unit Pa] and 15–11 ka [Unit Pb], Singer et al. 2008) basaltic to basaltic andesite lavas from the southern flank of the Puyehue edifice (Fig. 1) and surrounding minor eruptive centres (Table 1). Any adhering matrix or oxidised rind was removed by hand, and samples were then soaked in (frequently changed) milli-RO water for a minimum of 1 week to remove any soil horizon contamination within vesicles. Samples were then dried thoroughly at 100 °C prior to crushing. An aliquot of the sample was selected to mill, using a tema mill, to produce between 50 and 100 g of powder, for whole rock major, trace, and isotopic analyses. Major and selected trace elements were analysed by X-ray fluorescence (XRF) at the University of East Anglia (UEA) using a Bruker-AXS S4 Pioneer. Prior to analysis by inductively coupled plasma mass spectrometry (ICPMS) ~ 250 mg was weighed accurately into PFA vials. Samples were digested in 16 M HNO<sub>3</sub> (2 ml), 29 M HF (2.5 ml), and 12 M HClO<sub>4</sub> (1 ml) following standard dissolution techniques (see Supplementary Material 1 for full details). Samples were stored in LDPE bottles until day of analysis. A series of blanks and reference materials (BCR-2; SRM2711a and BGS102) were also prepared within the batch.

Samples were analysed for whole rock trace element concentrations using an Agilent 8900 series ICP-MS/MS fitted with a collision/reaction cell at the British Geological Survey (BGS). All elements were analysed using He as a collision gas except P, S, and As which used O<sub>2</sub> and Se which used H<sub>2</sub> as reaction gases. Full process quality control was provided by the digested reference materials and blanks. These blanks were used to define the batch detection limits (see Supplementary Material 1), and reference CRM-basalt run as a quality control was used to constrain precision and accuracy (see Supplementary Material 1). ICP-MS/MS batch control was ensured by the analysis of a series of chemical quality control standards covering the range of sample concentrations.

Radiogenic isotope analyses were undertaken at BGS. 150 to 200 mg of powdered sample was weighed and leached in 5 ml of 10% acetic acid at 60 °C for 2 h. After discarding the leachate, the samples were digested in 29 M HF and 16 M HNO<sub>3</sub> following standard dissolution techniques (see Supplementary Material 1 for complete methodology). Separation of Sr and Nd via column separation follows established ion exchange methods

**Table 1** Sample list and location/composition details

Sample	Eruptive centre	Lat	Long	Sample type	SiO <sub>2</sub> (%)	MgO (%)	CaO (%)	Na <sub>2</sub> O + K <sub>2</sub> O (wt.%)	<sup>87</sup> Sr/ <sup>86</sup> Sr	± 2SE	<sup>143</sup> Nd/ <sup>144</sup> Nd	± 2SE
VTL-01	Anticura	-40.664230	-72.155210	Lava	55.57	4.54	8.26	4.70	-	-	-	-
VTL-02	Anticura	-40.663670	-72.144920	Spatter	51.18	4.89	10.10	3.53	0.704074	0.000011	0.512852	0.000016
VTL-03	Anticura	-40.664830	-72.168300	Lava	55.21	4.70	8.36	4.59	0.703969	0.000009	0.512828	0.000009
VTL-05	Anticura	-40.661720	-72.14961	Bomb	51.23	4.84	10.13	3.62	-	-	-	-
VTL-10	Antillanca	-40.774585	-72.181876	Scoria	52.25	5.35	9.00	3.98	0.704055	0.000010	0.512842	0.000010
VTL-13	Antillanca	-40.779169	-72.171655	Scoria	50.99	6.60	9.16	3.52	0.704073	0.000006	0.512838	0.000008
VTL-18	Puyehue	-40.607616	-72.132525	Lava (prehistoric)	51.73	6.03	8.93	3.75	0.704078	0.000007	0.512831	0.000012
VTL-19	Puyehue	-40.607592	-72.131350	Lava (Pa ~ 43 ka)	51.81	5.61	9.55	3.70	0.704212	0.000011	0.512823	0.000011
VTL-20	Puyehue	-40.607366	-72.130651	Lava (Pb 15–11 ka)	52.54	5.29	9.03	3.86	0.704223	0.000009	0.512836	0.000009
VTL-25	Rupanco	-40.862781	-72.308370	Scoria	51.82	5.09	8.84	3.88	0.704065	0.000006	0.512850	0.000010
VTL-27	Carrán Los Venados	-40.369989	-72.043935	Scoria (Holocene)	51.54	4.43	7.95	4.07	-	-	-	-
VTL-29	Carrán Los Venados	-40.372796	-72.085158	Scoria (1907 CE)	52.4	4.05	7.65	4.40	0.704100	0.000012	0.512876	0.000011
VTL-30	Carrán Los Venados	-40.361104	-72.060113	Scoria (1979 CE)	51.9	4.26	7.83	4.23	0.704133	0.000011	0.512869	0.000009
VTL-31	Carrán Los Venados	-40.362233	-72.058676	Lava (1979 CE)	51.9	4.23	7.81	4.37	0.704108	0.000015	0.512870	0.000010

(see Supplementary Material 1 for complete methodology). Nd fractions were dissolved in 1 ml of 2% HNO<sub>3</sub> prior to analysis on a Thermo Scientific Neptune Plus mass spectrometer operated in static multicollection mode. Data are normalised to  $^{146}\text{Nd}/^{144}\text{Nd} = 0.7219$ . Four analyses of the JNd-i reference material gave a value of  $0.512085 \pm 0.000014$  ( $2\sigma$ ). Results are quoted relative to a value of 0.512115 for this reference material. Two analyses of the BCR-2 rock reference material run with the samples gave identical results of  $0.512646 \pm 0.000001$  ( $2\sigma$ ), compared to accepted values of  $0.512634 \pm 0.000012$  (Weis et al. 2006). Sr fractions were loaded onto outgassed single Re filaments using a TaO activator solution, and analysed in a Thermo-Electron Triton mass spectrometer in multi-dynamic mode. Data were normalised to  $^{86}\text{Sr}/^{88}\text{Sr} = 0.1194$ . Nine analyses of the NBS987 reference material gave a value of  $0.710257 \pm 0.000008$  ( $2\sigma$ ). Sample data was normalised using a preferred value of 0.710250 for this reference material. Two analyses of the BCR-2 rock reference material run with the unknown samples gave a value of  $0.705026 \pm 0.000002$  ( $2\sigma$ ), compared with published values of  $0.705019 \pm 0.000016$  (Weis et al. 2006).

### Mineral textures and compositions

Mineral textural observations and in situ analyses were carried out on polished thin sections. BSE images of thin-section mineral textures and olivine crystals for diffusion modelling were obtained at the University of Derby using a Tescan Vega 3 scanning electron microscope (SEM) and at the SEM Shared Research Facility at the University of Liverpool using a Zeiss Gemini 450 FEG-SEM. Major element analyses of major mineral phases were obtained by EPMA using a JEOL JXA 8230 system at the University of Leeds, using wavelength-dispersive spectrometry. Analytical conditions varied depending on the phase being analysed; for full details of conditions and precision and accuracy of EPMA data, see Supplementary Material 1.

### Thermometry

In the absence of glass in lava samples where minerals were analysed for thermometry, magmatic temperatures are modelled from various mineral phases and ‘melt’ which is assumed to be whole rock compositions, where equilibrium can be demonstrated. For all samples where mineral compositions were obtained, the olivine-melt thermometer of Putirka (2008, Eq. 22, as applied at Villarrica, Pioli et al. 2015) and the Ca-in-olivine thermometer of Shejwalkar and Coogan (2013) were used (following Morgado et al. 2017). For the olivine-melt thermometry, equilibrium between ‘melt’ (i.e. whole rock compositions) and olivine minerals

was tested; any analyses where  $K_{\text{D}(\text{Fe-Mg})_{\text{ol-liq}}} \neq 0.3 (\pm 0.03)$  were discarded (Putirka et al. 2007). Only core compositions with  $\text{Fo} \geq 70$  were used for Ca-in-olivine thermometry (following Morgado et al. 2017). For two samples, where clinopyroxene analyses were obtained, the clinopyroxene-whole rock thermometer of Neave and Putirka (2017, adapted from Putirka 2008, Eq. 33) was used (following similar application at other SVZ volcanoes: Namur et al. 2020; Vander Auwera et al. 2021; DeSilva et al. 2023; Oyarzún et al., 2022). The application of various thermobarometers here is limited by the available mineral phases. Whilst water has been shown to have an effect on the olivine-melt thermometry, past studies have shown that the PCCVC is relatively dry (Gerlach et al. 1988; Castro et al. 2013). For detailed review and development of thermobarometric assessments of magmatic conditions in the SVZ see Boschetty et al. (2022).

### Diffusion modelling parameters

To undertake diffusion modelling, orientations of olivine mineral grains were determined by electron back-scatter diffraction (EBSD) methods using a FEI Quanta 650 Field Emission Gun-Environmental Scanning Electron Microscope (FEGSEM) at the University of Leeds. Subsequently, greyscale profiles of Fe–Mg in olivine were extracted from BSE images using ImageJ® software. The greyscale values were tied to Mg# [ $\text{Mg\#} = 100 \times \text{Mg} / (\text{Mg} + \text{Fe})$ ] using analysed EPMA spots, and then modelled using AUTODIFF following the method of Couperthwaite et al. (2020). Modelling of boundaries from 81 crystals from Puyehue and 5 crystals from Anticura was undertaken at temperatures of 1110 °C, based on olivine-melt geothermometry (Putirka 2008),  $f\text{O}_2$  at the nickel-nickel oxide (NNO) buffer (following the approach of Morgado et al. 2017), and 200 MPa pressure (following MELTS modelling of phase stability, see results); however, pressure has only a minor effect on timescales (Morgado et al. 2017). Each Mg# profile was extracted perpendicular to the imaged crystal edge, and the orientation of this profile relative to crystallographic axes (established from output Euler poles in EBSD analyses, using the spreadsheet Eulerproc (Morgan pers. Comm., available on request)) was input into the AUTODIFF model to account for the known anisotropy of Fe–Mg interdiffusion in olivine (Couperthwaite et al. 2020). Uncertainties on modelled timescales were calculated using a Monte Carlo simulation incorporating a  $\pm 20$  °C uncertainty on temperatures (based on common uncertainties in olivine-melt thermometry (Putirka et al. 2007), and based on ranges in ol-melt modelled temperatures), and associated uncertainties on true pixel size, the number of integrated pixel lines across each boundary,  $f\text{O}_2$  uncertainty, and the greyscale values used to define the Mg# values. Absolute estimates of the uncertainty on modelled temperatures are limited by

available experiments that match our studied compositions and conditions of magmas at the PCCVC; however, variations in modelled  $T$  will systematically shift timescales as a series, as a unitary temperature has been used for all models; therefore, the relative differences in timescales will remain.

## Results

### Whole rock compositions

Fourteen samples of Puyehue and surrounding SEC were analysed to quantify their whole rock composition (Fig. 1; Table 1). All samples fall into the basalt and basaltic andesite fields (Fig. 2a), with  $\text{SiO}_2$  concentrations of 50.5–54.9 wt.%, MgO concentrations of 4.40–6.54 wt.%, and  $\text{Na}_2\text{O} + \text{K}_2\text{O}$  3.48–4.65 wt.%. Samples from Puyehue have restricted compositions on the basalt-basaltic andesite boundary (Fig. 2a), with MgO of 5.15–5.92 wt.%, and are at the least-evolved end of PCCVC samples previously published (Jicha et al. 2007; Singer et al. 2008; Fig. 2a).

Trace element concentrations are similar between Puyehue samples and other SEC (Fig. 2b), with trace element abundances, normalised to primitive mantle (Sun & McDonough 1989), for Puyehue showing higher abundances of HREE than the SEC. All samples studied (excluding VTL-27) show limited evidence for extended crustal residence, following the model of Cembrano and Lara (2009), with no difference in behavior of Rb vs. Cr concentrations between Puyehue mafic samples and the SEC south of the PCCVC (Fig. 2c). Samples from northern SEC (Carrán Los Venados field), are substantially different, with much lower Cr concentrations for any given Rb concentrations (Fig. 2c).

Eleven samples were selected for radiogenic Sr and Nd isotopic data collection, from Puyehue, Anticura, and other associated SEC (Fig. 1; Table 1). All of the samples have isotopic ratios between 0.703969 and 0.704223 for  $^{87}\text{Sr}/^{86}\text{Sr}$ , and 0.512823 and 0.512852 for  $^{143}\text{Nd}/^{144}\text{Nd}$ , and hence lie within the CSVZ and SSVZ field defined by Hickey et al. (1986) and Hickey-Vargas et al. (2016a) (Fig. 2d). Puyehue samples have slightly more radiogenic  $^{87}\text{Sr}/^{86}\text{Sr}$  (and less radiogenic  $^{143}\text{Nd}/^{144}\text{Nd}$ ) than the samples from SEC (Fig. 2d). For full data set, see Supplementary Material 2.

### Petrography and mineral chemistry

All samples studied contain varying proportions of olivine (~12–27% of the thin section) and plagioclase feldspar (~54–69% of thin section) as macrocrystic phases (see Supplementary Material 3, with modal % of mineral phases present). Samples typically contain between 15 and 75% macrocrysts. Spatter and lava samples have a holocrystalline to hypocrystalline groundmass (Fig. 3a) whereas samples

of tephra often have glass preserved in the groundmass (Fig. 3b). Alongside macrocrystic olivine and plagioclase feldspar, minor proportions of pyroxenes (ortho- and clinopyroxene), titanomagnetite, and Cr-spinel are variably present within the groundmass. Samples from all studied SEC and Puyehue have euhedral to subhedral olivine and plagioclase macrocrysts; however, Puyehue samples distinctively preserve high-Fe rims on many olivine crystals (Fig. 3c with rims appearing bright in BSE imagery). High-Fe rims are only rarely developed in Anticura samples (Fig. 3d), and are absent in samples from all other SEC studied here (Fig. 3b). The bright rim on olivine grains is not ubiquitous for all olivine macrocrysts of Puyehue samples, nor all crystal faces of a single grain; within a single crystal, the high-Fe rim can be seen to not develop where smaller crystals are attached to the macrocryst face (Fig. 3c), whereas immediately adjacent to the attached crystal, the high-Fe rim is observed. This has important implications for the timing of rim development and the processes that can be traced with diffusive chronometry of this zoning. Samples from the SEC studied here have variable mineral textures, with historic Carrán Los Venados samples having much smaller mineral grains, characteristic skeletal morphology olivine grains (Fig. 3e). Minerals in all SEC lack well-developed zonation (Fig. 3f).

Puyehue macrocrysts show distinct normal zoning with respect to both plagioclase and olivine compositions, with rims having overlapping and more evolved compositions than cores or groundmass: olivine cores have Fo# of 73–83 and NiO concentrations of 0.04–0.13 wt.%, compared with rims of Fo# 58–82, and NiO concentrations of 0.02–0.11 wt.% (Fig. 4a). Rare antecrysts (here used to signify crystals that are related to the magma system, but not in equilibrium with their host magma) are present with cores of Fo#85, and rims of Fo#87–88 (Fig. 4a). Plagioclase cores are An73–An88, rims expand this range to An38–An88, and groundmass feldspar is An52–An82 (Fig. 4b). Minor clinopyroxene present shows no systematic difference between core and rim analyses, but variable grain compositions, with 5 grains having Mg# 45–67.

Anticura plagioclase are similar to Puyehue, with less-evolved cores of An80–An91, variable, and overlapping rim compositions of An51–An91 and intermediate groundmass of An47–An79 (Fig. 4b). Compositions of Anticura olivine are similar to those of Puyehue (with core olivine having Fo# 78–82, NiO 0.00–0.11 wt.%), although rim compositions are slightly more restricted than those of Puyehue (Fo# 60–77, NiO 0.00–0.08 wt.%; Fig. 4a). Two clinopyroxene crystals had no difference in composition between cores and rims, with Mg# of 43–46. Compositions of Puyehue and Anticura mineral phases encompass the entire range of the entire sample suite both from Puyehue and all SEC studied in detail here (Fig. 4). For full data set, see Supplementary Material 2.

**Fig. 3** Compiled BSE images of olivine from various PCCVC and SEC samples showing the range of olivine textures preserved. (a) Anticura spatter sample showing the presence of glomerocrysts of olivine, plagioclase and clinopyroxene. (b) Antillanca proximal SEC olivine with glassy groundmass, and no compositional change across olivine macrocryst. (c) Puyehue olivine showing the development of a high-Fe rim, following the growth of the smaller macrocrysts attached to the olivine crystal. (d) Anticura olivine with the rare high-Fe rim, with significantly narrower width than Puyehue in (c). (e) Skeletal morphology olivine and FeTi oxide in Carrán Los Vendados scoria and lavas. (f) Unzoned plagioclase feldspar from Carrán Los Venados. Red line in all images is 200  $\mu\text{m}$  in length

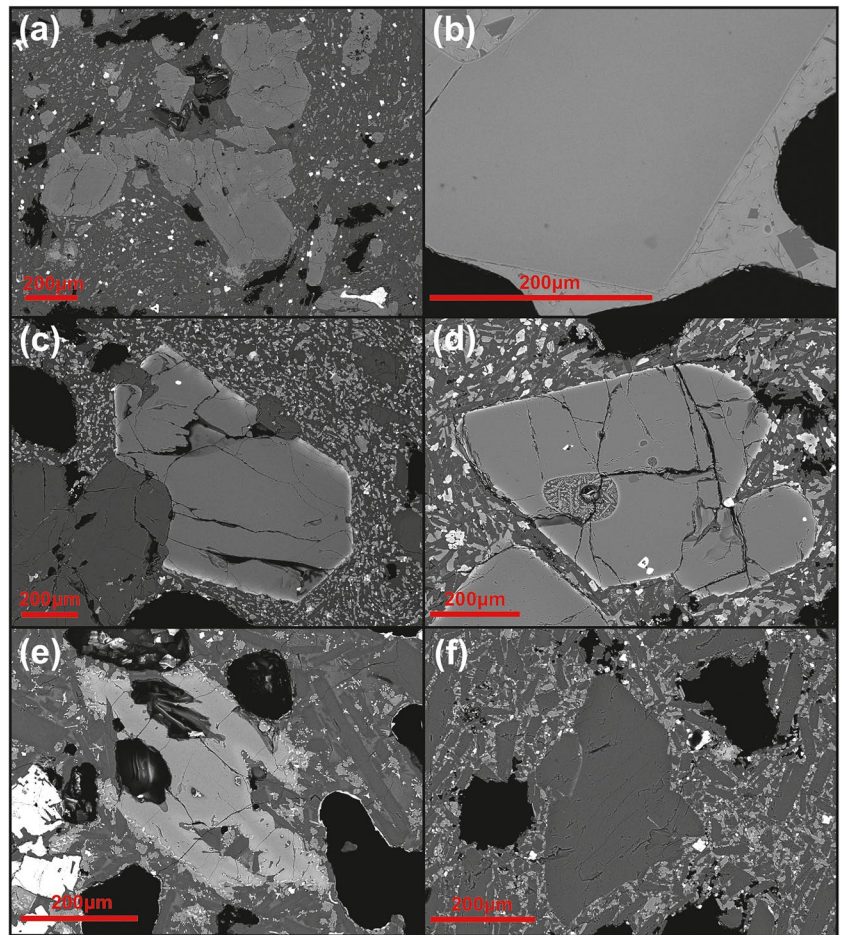
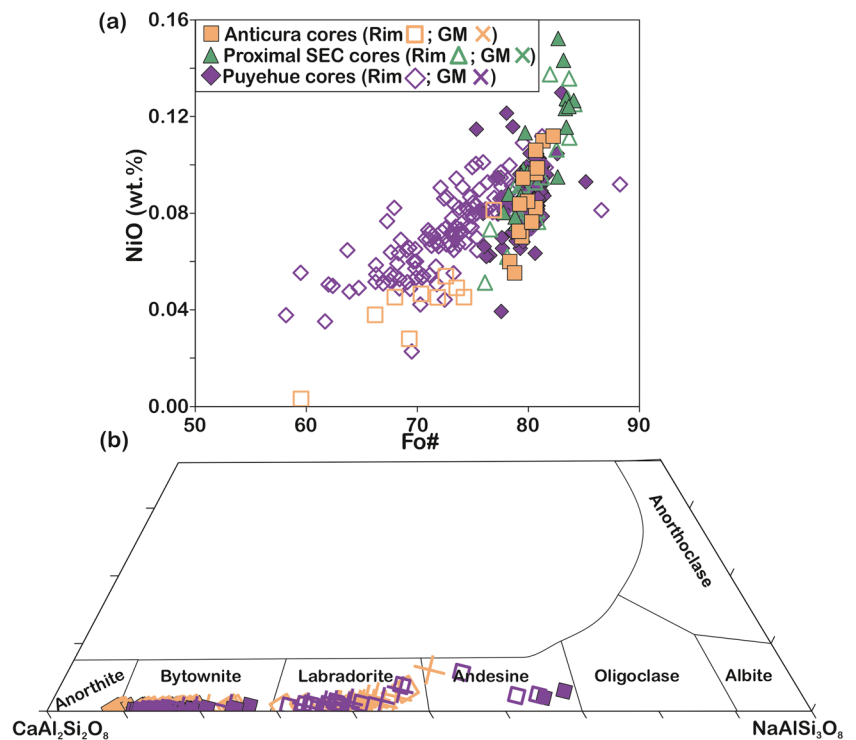


**Fig. 4** Olivine (a) and plagioclase (b) major element compositions from the Puyehue (purple diamonds), Anticura (orange squares), and SEC proximal to Puyehue (green triangles). Core analyses are filled symbols, rim analyses are hollow symbols, and groundmass crystals are colored crosses



## Intensive variables

Estimation of intensive variables is limited by the available mineral phases and the lack of glass in most samples studied here. Olivine-melt thermometry yields no significant differences in modelled temperatures between cores and rims of olivine in either Puyehue or Anticura minerals. Puyehue olivine-melt models give a mean temperature of 1120 °C ( $n=32$ ). Six clinopyroxene-whole rock pairs gave a similar average temperature of 1098 °C, but Ca-in-olivine thermometry gave an average of 1036 °C ( $n=37$ , Table 2). Similarly, Anticura olivine-melt and clinopyroxene-whole rock thermometry produced higher average temperatures (1158 °C,  $n=3$ ; 1102 °C,  $n=4$ , respectively) than those obtained from Ca-in-olivine thermometry (average  $T=1058$  °C,  $n=6$ ; Table 2). The Ca-in-olivine thermometer is calibrated for systems where olivine is in equilibrium with both a clinopyroxene and a low-Ca pyroxene phase (Shejwalkar and Coogan 2013); however, neither pyroxene phase is abundant in the samples studied here. In the absence of a co-saturated Ca buffer, the Ca-in-olivine temperatures can be considered minima, which explains why these values are lower than those modelled using olivine/cpx-melt thermometry. Thus, the higher temperatures produced by olivine/cpx-melt thermometry are expected to reflect the true magmatic temperatures of these mafic melts more appropriately.

## Diffusion chronometry

Fe–Mg diffusion modelling was undertaken on three samples that preserved Fe–Mg zonation, one from Anticura (VTL-02), and two from Puyehue (VTL-19, VTL-20) where Fe-rich rims were more extensively preserved. All modelling was carried out at constant  $T$ ,  $P$ , and  $fO_2$  (see ‘Methods’ section). Upon extracting greyscale profiles from BSE images,

only a single sample (VTL-19) had compositional gradients representative of solely diffusional relaxation, with good fits to the models, and no obvious systematic deviation from simple, fixed-boundary isothermometric diffusion identified. Both VTL-02 (Anticura) and VTL-20 (Puyehue) have compositional gradients that deviate from simple diffusion models at the shallowest gradients (at highest  $Fo$  contents) where the profile curves away from the model. This is evidence of processes affecting the profiles that are not purely those of diffusive exchange of Fe–Mg at constant temperatures. Previous studies of such deviations between model and natural profiles have demonstrated the importance of crystal growth and changing temperatures in their origin (Couperthwaite et al. 2021, 2022; Kahl et al. 2023). A similar analysis of growth and temperature variations in our samples would require the equilibrium liquid composition to be known, and in the absence of such data cannot be currently undertaken. Instead, we stress that the limitations of simple modelling should be borne in mind when considering the significance of any modelled timescales (see the ‘Implications of diffusion timescales’ section in the ‘Discussion’ section).

Sample VTL-19 from Puyehue yielded 54 crystals across which diffusion could be modelled (for example, see Fig. 5a, b, full data set Supplementary Material 4). One hundred diffusion models were applied, and where multiple profiles within a single crystal were modelled, the profile which showed the best fit and/or the shortest timescales was used as the final timescale for that crystal. Modelled timescales range between 1.8 and 57 days (Fig. 6), with variable  $\Delta Fo$  across the modelled boundary of between 0.9 and 23.6 Mol%, and average  $\Delta Fo$  of 8.3 Mol% across the modelled boundary.

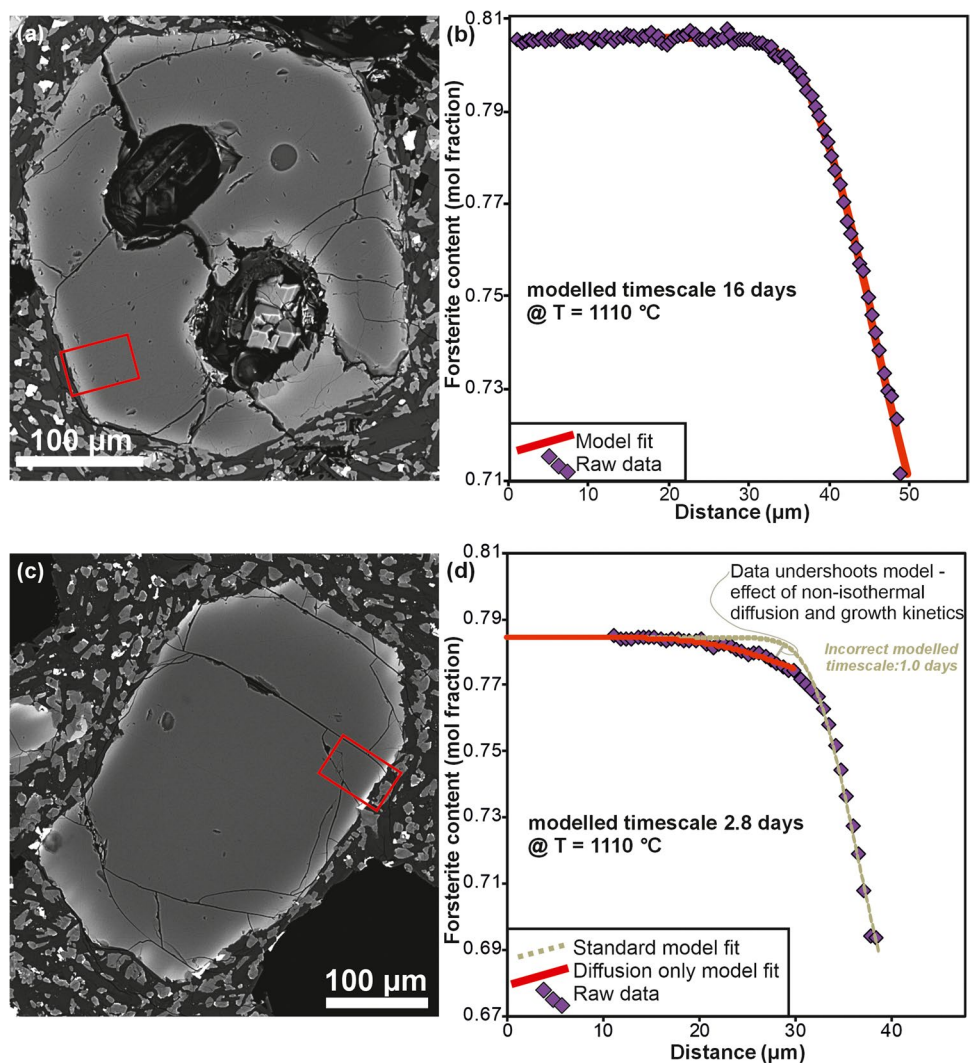
Sample VTL-20, also from Puyehue, yielded 27 crystals across which diffusion could be modelled. However, VTL-20 contained boundaries that exhibited a combination

**Table 2** Thermometry results

Sample	Eruptive centre	Method	Average T (°C)	$n$	Minimum T (°C)	Maximum T (°C)	uncertainty on individual model T (°C)
VTL-02	Anticura	ol-melt <sup>1</sup>	1158	3	1106	1184	±15
VTL-02	Anticura	Ca-in-ol <sup>2</sup>	1058	6	1049	1067	±30 <sup>2</sup>
VTL-02	Anticura	cpx-WR <sup>3</sup>	1102	4	1040	1136	±30
VTL-10	Antillanca	Ca-in-ol <sup>2</sup>	1058	6	1043	1068	±30 <sup>2</sup>
VTL-13	Antillanca	ol-melt <sup>1</sup>	1160	13	1154	1164	±15
VTL-13	Antillanca	Ca-in-ol <sup>2</sup>	1051	2	1037	1065	±30 <sup>2</sup>
VTL-19	Puyehue	ol-melt <sup>1</sup>	1129	16	1116	1139	±15
VTL-19	Puyehue	Ca-in-ol <sup>2</sup>	1034	20	1009	1055	±30 <sup>2</sup>
VTL-20	Puyehue	ol-melt <sup>1</sup>	1111	16	1106	1118	±15
VTL-20	Puyehue	cpx-WR <sup>3</sup>	1098	6	1089	1117	±30
VTL-20	Puyehue	Ca-in-ol <sup>2</sup>	1038	17	1025	1053	±30 <sup>2</sup>

<sup>1</sup>: Eq. 22 Putirka (2008); <sup>2</sup>: Shejwalkar and Coogan (2013); <sup>3</sup>: Neave and Putirka (2017)

**Fig. 5** Examples of the zonation preserved in olivines from VTL 19 (a, b) and VTL 20 (c, d). Compositional profiles extracted from BSE images in the red zones on (a, c) are shown in (b, d) where BSE intensity is calibrated to EPMA compositions. Extracted profiles are in purple with modelled profiles in red. In (d), the clear undershoot of the extracted profile at the apex of the gradient, when the full zone is considered, is evidence of coupled growth and diffusion and a probable changing boundary condition due to changing temperature (see examples in Couperthwaite et al. (2020) and Kahl et al. (2023)); instead, a curtailed profile is modelled where a pure diffusion component can be modelled, indicating stalling and storage prior to late-stage ascent and growth of the final section of the high-Fe rim is seen



of growth (likely within a cooling lava flow) and diffusional relaxation (Fig. 5c, d, Supplementary Material 4), so in order to remove the growth effect, diffusion was modelled only to the inflection in profile gradients (Fig. 5d, following the method of Couperthwaite et al. 2020). Similar to VTL-19, 27 crystals yielded 41 diffusion models, but only profiles which showed the best fit and/or the shortest timescales were used as the final timescale for each crystal. Modelled timescales range between 1.4 and 47 days (but only one crystal yields timescales > 23 days; Fig. 6), with variable  $\Delta Fo$  across the modelled boundary of between 0.7 and 10.2 Mol%. Average  $\Delta Fo$  across the modelled boundary was 2.0 Mol%.

Finally, only five crystals in the Anticura sample preserved high-Fe rim zonation, and all showed evidence of significant growth (presumably synchronous and subsequent to eruption), so all timescales modelled are considered maxima. For the five crystals where standard diffusion modelling was applied, timescales varied between 1.5 and 8.4 days for the formation of the rim (Fig. 6, Supplementary Material

4), with  $\Delta Fo$  across the modelled boundary of between 4.2 and 16.6 Mol% (with the average  $\Delta Fo$  being 11.0 Mol%). However, the evidence of growth during diffusion means that these timescales should be interpreted with caution.

## Discussion

### Magmatic evolution of mafic magmas at PCCVC

Extensive work has been carried out on the production and evolution of mafic magmas of the SVZ (for review, see Hickey-Vargas et al. (2016a) and references therein), and has shown that significant variations in composition of SVZ basalts and basaltic andesites along-strike of the arc are a function of varying crustal thicknesses and role of the LOFS in facilitating magma ascent (López-Escobar et al. 1995; Cembrano & Lara 2009; Hickey-Vargas et al. 2016a). On more local scales, contrasting La/Yb ratios between

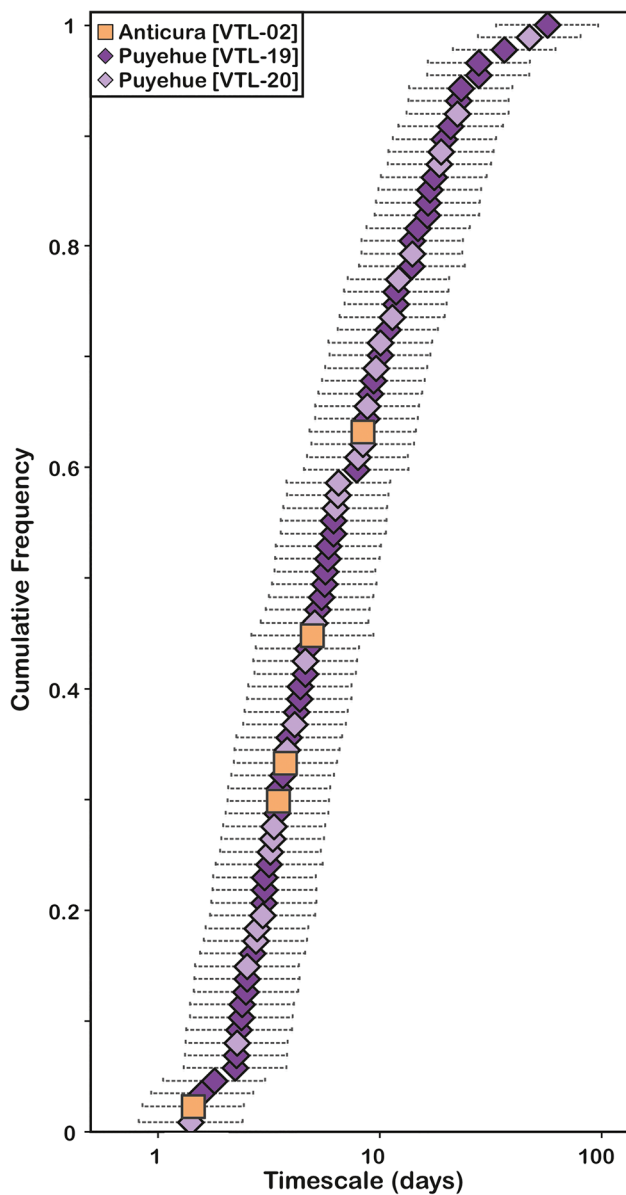


**Fig. 6** Compiled timescales of Fe–Mg interdiffusion modelling from zoned olivine crystals in Puyehue and Anticura lavas. Uncertainty bars represent combined uncertainty at 1 s.d. (see the ‘Methods’ section for details)

stratovolcanic edifices and proximal SEC have been inferred to represent varying degrees of interaction with lithospheric pyroxenite (e.g. Hickey-Vargas (2016b)).

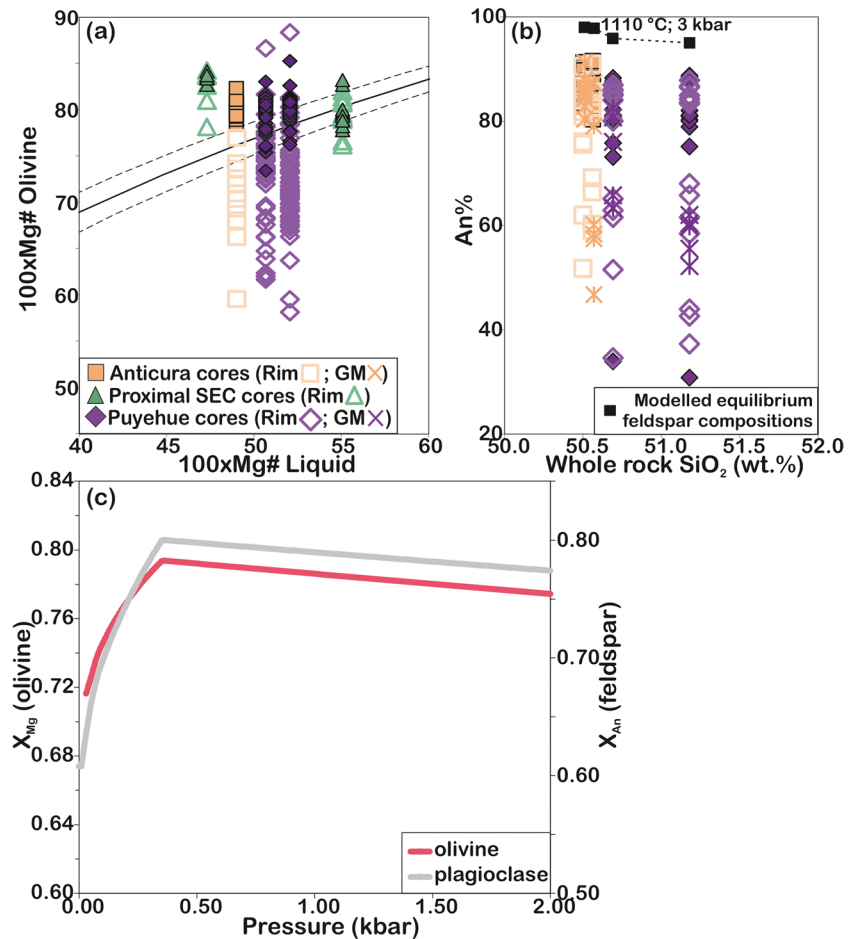
Whilst detailed petrographic and geochemical study of PCCVC stratovolcanic products has led to the suggestion that both closed-system fractional crystallization and magma mixing contribute to the evolution of intermediate and felsic magmas (Gerlach et al. 1988; Singer et al. 2008; Jicha et al. 2007), the relationship between mafic parental magmas of the PCCVC and the surrounding SEC, and the role of crustal stress states in facilitating magma ascent, can be

further examined. Therefore, understanding the role (if any) of stalling, fractional crystallization, and magma mixing in producing the basaltic magmas studied here will allow both the early stages of magmatic evolution at the PCCVC to be constrained, and thus at what stage the high-Fe rims are developed in the Puyehue olivine grains.

As has been well-documented throughout the SVZ (e.g., Jicha et al. (2007); Singer et al. (2008)), the mafic magmas of the PCCVC and SEC are not primary, mantle-derived basalts. Low MgO and Ni concentrations (Fig. 2) are not consistent with being a primary, mantle-derived partial melt, and thus lower crustal fractionation of phases including olivine, titanite, and clinopyroxene is likely to have occurred (cf. Pioli et al. 2015; McGee et al. 2017; Winslow et al. 2020, 2022). This fractionation did not involve amphibole or garnet, as there is no evidence for depletion in MREE or HREE when compared with other centres in the SVZ (Fig. 2b). Unlike at other stratovolcanoes in the SVZ, there are also no systematic differences in La/Yb ratios between Puyehue basalts and their surrounding SEC studied here. Similarly, radiogenic isotopic data shows no distinction between Puyehue and SEC (Fig. 2d). These lines of evidence all suggest that the mafic magmas erupted from both Puyehue and surrounding SEC are typical of the Central SVZ (Hickey-Vargas et al. 2016a), and share similar origins and lower crustal evolution prior to their eventual eruption.

Nonetheless, variations between eruptive centres are evident in the mineral textures, phase abundances, and compositions (Figs. 3, 4), and macrocrystic phases are present, which suggest some stalling and mineral growth (or crystal accumulation) prior to eruption. In both samples from Puyehue (and one from Antillanca, a southern proximal SEC, Table 1), olivine core compositions overlap with the equilibrium field for their whole rock compositions, with rims extending to lower Fo than is in equilibrium with the whole rock (Fig. 7a). In Anticura samples, and a second proximal SEC sample, core compositions are less-evolved than their host whole rock compositions, suggesting that these minerals are accumulated from prior fractionation processes, or have had time to equilibrate to lower Fo concentrations produced through fractionation during prolonged storage (cf. Winslow et al. 2022). Rim compositions trend towards (and past) the lower Fo values suggested from whole rock compositions (Fig. 7a). Texturally, olivine crystals in Puyehue basalts are euhedral to subhedral, whereas olivine crystals in Anticura samples are solely subhedral and often occur as glomerocrysts, suggesting the incorporation of antecrystic material or mush into an ascending melt (e.g. Holness et al. (2007), Neave et al. (2013), and Winslow et al. (2022)). By contrast to olivine, no plagioclase crystals seem to be in chemical equilibrium with their host whole rock (Fig. 7b), yet euhedral tabular morphologies are observed (Fig. 3), suggesting there are some challenges with interpreting

**Fig. 7** Variation in olivine (a) and plagioclase (b) compositions with whole rock Mg# (a) or SiO<sub>2</sub> (b) and the calculated equilibrium compositions of the respective crystal phases based on whole rock XRF data (Table 1, and Supplementary Material 2). Cores are filled symbols, rims are open symbols, and groundmass minerals are crosses. In (b), equilibrium compositions of feldspar are calculated at 1110 °C and 3 kbar. This is compared with modelled mineral compositions (c) of olivine (red line) and plagioclase (grey line) during isothermal decompression from rhyolite-MELTS modelling (Gualda & Ghiorso., 2015)



equilibrium solely from textures or ‘melt’-crystal chemical exchange when there is evidence for accumulation of minerals. For some plagioclase cores to be in equilibrium with their host whole rock, it would require higher pressure (~5 kbar) and lower temperatures (~1000 °C) conditions which are not evidenced in any other mineral phase in these samples.

To determine likely stalling depths for mineral formation, MELTS modelling of mineral fractionation (version 1.2.0: Gualda & Ghiorso 2015) was undertaken using the whole rock composition of VTL-19 (least-evolved sample) as a starting composition, and 1.5 wt.% H<sub>2</sub>O (following inferences of dry magmas at Puyehue: Gerlach et al. 1988; Castro et al. 2013; Oyarzún et al. 2022). At pressures  $\geq 2.8$  kbar clinopyroxene is the favored ferromagnesian phase; only at lower pressures is olivine the fractionating ferromagnesian phase. Given the absence of a pressure-sensitive phase, the pressures of stalling can only be constrained to between ca. 2.7 kbar (from MELTS modelling) and 1.2 kbar (equivalent to the 5 km intracrustal discontinuity inferred to be shallowest stalling, Tassara and Echaurren (2012)), equating to olivine crystallization between approximately 5 and 11 km depth

(it should be noted that slightly lower water concentrations would expand the stability of olivine to slightly higher pressures).

Subsequent to mineral core formation (at higher-Fo), the low-Fo rim observed in Anticura and Puyehue olivine developed. These low-Fo rims are not in chemical equilibrium with their whole rock compositions (Fig. 7). MELTS modelling of in equilibrium crystallization mode as no minerals are removed from the magma, starting from measured whole rock compositions during isothermal decompression from 2 kbar to surface (at a starting temperature of 1110 °C, and assuming 1.5 wt.% H<sub>2</sub>O) only yields olivine of Fo 71.6 (Fig. 7c). These low-Fo rims could be explained by mixing with a less-evolved magma (cf. Leeman & Smith 2018; Oeser et al. 2018) yet no other mineral phases record evidence of this interaction (Figs. 3, 4), whole rock compositions are limited (Fig. 2), and olivine cores are in equilibrium with the whole rock (Fig. 7a). Instead, this large difference in Fo between cores and rims is more likely to represent disequilibrium growth during (or subsequent to) ascent (cf. Couperthwaite et al. 2020, 2021). By applying diffusion chronometry to the zonation preserved in these olivine crystals, the timescales

associated with rim formation (and inferred ascent and/or post-eruptive growth and quench) can be constrained.

### Implications of diffusion timescales

The preservation of well-developed normal rims on olivines, and comparable compositions of mineral phases and whole rock measurements from samples VTL-19 and VTL-20 implies similarities in magmatic processes between the two mafic eruptions from Puyehue, at ~43 ka (VTL-19) and 15–11 ka (VTL-20). However, only sample VTL-20 has evidence for systematic growth affecting the outermost rims of olivine crystals, despite it being a younger sample where the rubbly lava tops are better preserved for sampling of rapidly cooled material. The evidence of clear two-stage processes in the eruption of unit Pb (Table 1, Singer et al. 2008) suggests that magma stalled in the crust for a period of ~days to a few weeks prior to final ascent and eruption to form the lava flow sampled in this study. Contrary to this, there is no evidence for stalling on ascent in sample VTL-19 (from unit Pa, Singer et al. 2008), where timescales are likely to represent growth of rims on ascent from deeper storage to eruption, taking on the order of days (>90% of modelled profiles have timescales <10 days). Both of these timescales are short compared with other stratovolcanoes (e.g. days to years at Etna, Kahl et al. 2011; weeks to years at Llaima, Ruth et al. 2018), and could be considered maxima, due to the potential for extended diffusion occurring following eruption which affects lava flow samples and extends apparent timescales in lavas relative to co-erupted tephra (Conway et al. 2020; Couperthwaite et al. 2021, 2022). These observations imply that signs of unrest prior to any future mafic eruptions will occur only shortly before eruption (~days, if unrest signals are detectable as soon as ascent begins), similar to that seen in historical eruptions from the Canary Islands (e.g. 2021 eruption of La Palma: Global Volcanism Programme 2021; historical eruptions on Tenerife: Albert et al. 2015), and longer than that observed prior to the silicic 2011–2012 eruption of Cordon Caulle (Basualto et al. 2023).

SEC olivine crystals studied here either have little to no preserved zonation or show evidence for rapid growth in highly undercooled magmas (Fig. 3a, e), all suggesting that even more rapid magma ascent occurs in centres lacking a large stratovolcanic edifice (cf. McGee et al. 2017; Morgado et al. 2017 for comparisons with SEC around Villarrica). These observations imply that future monogenetic eruptions in the PCCVC region may not be preceded by many—or any—days of detectable unrest, and thus suggest a noteworthy hazard associated with the SVZ. Where zonation is preserved, timescales modelled are on similar orders of magnitude (but at the shorter range) as Puyehue samples. However, there is again evidence that this zonation is a product of late-stage growth within the cooling magma, because zonation

is not developed around attached microlites (Fig. 3c, cf. Winslow et al. 2022), and extracted profiles systematically undershoot the modelled inflection point (Fig. 5d). These profile shapes are similar to examples from Hawai'i and Piton de la Fournaise (Couperthwaite et al. 2020, 2021, 2022) and those present in lunar basalts (Bell et al. 2023), suggesting this is not an uncommon phenomenon.

There is clear evidence of the impact on diffusional relaxation from cooling within lava flows, as has been highlighted by previous authors (e.g. Conway et al. (2020) and Couperthwaite et al. (2020)). Despite sampling of rubbly lava surfaces or spatter, this cooling effect could not be completely mitigated. Therefore, unless additional modelling (incorporating liquid compositions, cf. Couperthwaite et al. 2022) is undertaken, the data presented here suggest that lava flows cannot be guaranteed to preserve diffusion compositional profiles solely related to subsurface magmatic processes, and care should be taken when applying diffusion chronometry to lava samples, irrespective of how old the eruptions are, and where in the lava sequence samples are obtained (cf. Couperthwaite et al. 2022). In particular, careful assessment of the applicability of diffusion geospeedometry should be undertaken when compositional profiles are extracted. The deviation between the model and extracted profiles in this study was only evident from high spatial resolution profiles, and likely would have not been as obvious on an EPMA traverse. Diffusion chronometry is a valuable tool to understand subsurface magmatic timescales, yet it should be applied with caution.

### Variations in timescales and textures

Whole rock compositions and isotope ratios can be used to determine whether the source composition and melting dynamics are comparable across the PCCVC and surrounding SEC, to assess the potential impact changing magma genesis may have on magma ascent timescales. Magmas erupted from PCCVC and the surrounding SEC share similarities in whole rock compositions (Fig. 2), with some Anticura samples extending to slightly more evolved basaltic andesite (Fig. 2a), with accompanying higher incompatible trace element concentrations (Fig. 2b) and lower Cr (Fig. 2c). Yet, despite small variations, all samples have comparable radiogenic isotope ratios (Fig. 2d cf. McGee et al. 2017) suggesting that the magmas erupted in this region are from the same mantle source, with similar degrees of partial melting and crustal contamination. Similarly, compositions of olivine cores from Puyehue, Anticura, and surrounding SEC are overlapping (Fig. 4), again suggesting similarities in lower crustal evolution and growth of mineral phases. Yet, despite the similarities in whole rock and mineral compositions, and inferred source and lower crustal dynamics, there exist differences in mineral habits and zonation between Puyehue

and Anticura and the surrounding SEC. Therefore, the origin of these differences should be explored to understand late-stage magmatic processes and how the timescales associated with these processes may differ.

Puyehue (in compression and erupted through a  $> 70 \text{ km}^3$  polygenetic stratocone) mafic lavas contain euhedral olivine with well-preserved normal zonation, interpreted to reflect growth during ascent (and subsequent cooling in lava flows), whereas SEC Anticura samples (along the LOFS) have euhedral to subhedral olivine crystals without extensive zonation. Where normal zonation is evident in Anticura samples, these have shorter modelled timescales (less than 8.4 days) than those from Puyehue (less than 57 days, Fig. 6), and may have a greater component of growth within a lava flow (see the ‘Implications of diffusion timescales’ section and cf. Coup-erthwaite et al. 2021, 2022), suggesting that the majority of diffusive relaxation may have occurred during lava flow emplacement rather than ascent. The lack of rim formation prior to eruption at Anticura suggests that magma ascent is more rapid than at Puyehue, i.e.  $< 8$  days. Notably, samples from the Carrán-Los Venados SEC (extensional domain) have skeletal and hopper morphologies (Fig. 3e), indicative of rapid growth of olivine in high degrees of undercooling (Donaldson 1976; Faure et al. 2003), implying even shorter crustal residence for these magmas than compared with both Anticura, and Puyehue, and accompanying rapid ascent. The relationship between longer periods of transit at stratovolcanoes vs. shorter crustal transit times at associated SEC follows trends seen in other locations in the SVZ (e.g. Morgado et al. 2017), yet timescales modelled here from the PCCVC are substantially shorter than these past studies.

By integrating these petrological interpretations with known stress states the effect of stress state on controlling magma ascent in the PCCVC and surrounding SEC can be assessed. Reviews of magmatic ascent in brittle rocks, as dykes, highlight that the main controls on magmatic ascent are the key physical properties of magmas, interaction with pre-existing cracks and lithological changes, and the external stress field (Rivalta et al. 2015). In the PCCVC and surrounding SEC, physical properties (magmatic source dynamics, compositions, and temperatures), broad-scale lithologies, and crustal thicknesses are constant (see the ‘Magmatic evolution of mafic magmas at PCCVC’ section, Singer et al. 2008 and references therein); therefore, interaction with pre-existing structures and the external stress field are likely to exert the major control on variable magmatic ascent rates in this region. Extensive work to assess current local tectonics in the area shows that Puyehue is in relative compression (therefore inhibiting magmatic ascent and favoring subhorizontal ‘dyke’ formation), Anticura is in relative transpression (and is located above the LOFS master fault), and other SEC including Carrán Los Venados are in relative extension (Lara et al. 2006a). However, the local

stress field is a combination not just of regional tectonics, but also the topographic loading of the edifice(s) (Pinel & Jaupart 2000; Roman & Jaupart 2014; Davis et al. 2021). Without bespoke models, the relative importance of edifice load and tectonic forces and structures on ascent rate cannot be assessed here; however, the petrological constraints on timescales of mafic magma ascent at PCCVC and surrounding SEC support existing models that suggest both edifice load and local tectonic forces play a role in magma ascent in this region:

- 1) Variations in mineral textures between SEC (all lacking a large edifice) highlight the importance of local tectonics in controlling magma ascent. Carrán Los Venados (in transtension) has much more rapid transit of magmas through the crust than Anticura (in transpression).
- 2) Mafic magmas ascend more rapidly at Anticura (transpression) than at Puyehue (compression, stratocone), likely a combination of both local tectonics (e.g. Zellmer et al. (2014)) and the edifice effect (e.g. Roman and Jaupart (2014)). The evolution of mafic magmas to more evolved rhyodacites (Singer et al. 2008; Jicha et al. 2007; Winslow et al. 2022) at Puyehue (not seen at other SEC in the area) again highlights the long durations of storage at volcanoes in relative compression.

### Regional controls on polygenetic vs monogenetic volcanism

This study has shown that even where magma source and lower crustal dynamics are inferred to be similar, differences exist in upper crustal plumbing systems and ascent rates. Similar differences between polygenetic and monogenetic volcanic systems (or SEC generation, albeit with greater complexity) have been observed in other regions of the SVZ. In general, monogenetic volcanoes aligned with the LOFS have been shown to be less degassed, with higher Cl and S concentrations, than other SEC and stratovolcanic structures, which has been inferred to relate to more rapid magma ascent facilitated by the LOFS (Wehrmann et al. 2014). Specific examples of tectonic controls on magma ascent have been suggested in the Descabezado Grande Volcanic Field (DGVF) where rare, near-primitive mafic melts have been shown to reach shallow crustal levels (Salas et al. 2017, 2021) despite thicker crust in the northern end of the SVZ ( $\sim 33\text{--}36^\circ \text{ S}$ , Tassara & Echaurren 2012) and the absence of the LOFS (Cembrano & Lara 2009). Previous workers have suggested that more rapid (3.5–40 days) mafic magma ascent in these intermediate-felsic dominated volcanic areas (with extended crustal processing, Cembrano & Lara 2009) is facilitated by the presence of deep crustal structures (Salas et al. 2017, 2021).

In the Villarrica area (just ~145 km north of the PCCVC), again polygenetic stratovolcanoes (Villarrica, Quetripilán and Lanín) align along NW-trending structures whilst mafic SEC adjacent to these centres are either atop of the LOFS (and carry a pristine mantle signature) or lying outside (and are more similar to the stratovolcanoes) (Morgado et al. 2015, 2017; Hickey-Vargas et al. 2016a, b; McGee et al. 2017). However, this area has much more complexity in the magma source region, with diversity in radiogenic isotope ratios and degrees of light rare earth element (LREE) enrichment being used to infer heterogeneous mantle source regions and variable roles of pyroxenite in the mantle (Hickey-Vargas et al. 2016b) and/or increasing degrees of crustal contamination (McGee et al. 2017) when comparing between SEC and polygenetic volcanoes, but also within the various SEC. Mineral-specific studies have highlighted that SEC in the Villarrica region, similar to the SEC studied here, do not show evidence for shallow storage (unlike at the stratovolcanic edifices)—suggesting that the LOFS and low magma fluxes have prevented establishment of complex magma plumbing systems in this area (Morgado et al. 2015; Pioli et al. 2015; Boschetty et al. 2022). Work on the Caburgua SEC has modelled timescales of magma ascent which extend to significantly longer timescales than modelled for all PCCVC centres (up to 471 days, Morgado et al. 2017), with no comparisons yet published for stratovolcanic edifices or other SEC in the area.

The PCCVC has shown that timescales of magma ascent in the region are controlled by the crustal stress state (likely a combination of edifice load to some extent and local tectonics especially), with no difference in magma source regions (Fig. 2) and lower crustal stalling (Fig. 4). However, further work deconvolving the effect of upper crustal stress states, magma flux, and mantle melting regimes on magma ascent dynamics is required to apply this methodology to the wider SVZ.

## Conclusions

Combining whole rock geochemical data, in situ mineral analyses and petrographic observations of Puyehue and surrounding SEC can allow comparisons of magma generation, evolution, and ascent dynamics to be assessed within the context of variable upper crustal stress states and topography. Whole rock major, trace, and isotopic data show the similarities in magma generation processes at Puyehue and the surrounding SEC, with cryptic evidence for lower crustal evolution indicated by low MgO and Ni concentrations, which are not in equilibrium with mantle-derived primary melts. Yet, differences in mineral textures, equilibrium relationships, and modelled diffusion timescales between Puyehue stratovolcano and the

Anticura eruptive centre imply that there is variation in how magmas evolving in the lower crust ascend and erupt in the Puyehue region.

Of the studied samples, only Puyehue and Anticura samples have normal-zoned lower Fo rims developed on olivine grains. These disequilibrium rims developed during ascent and lava-flow emplacement as shown by the groundmass-rim textural relationships and equilibrium modelling of olivine rim compositions. Timescales of rim formation are shorter (days) in the sample from Anticura, reflecting formation only after eruption, whereas timescales are on the order of days to weeks in Puyehue samples, showing slower ascent than in the nearby SEC and possible shallow stalling. The differences in timescales resolved using petrology confirm the inferences from past workers that volcanic centres under different upper crustal stress states have different mafic magma ascent timescales, as geochemical assessments of the generation and evolution of the magmas studied here show no distinct differences. Compressional upper crustal stress states, and the impact of an established edifice likely inhibit mafic magma ascent at Puyehue, where sill-like storage would be favored at mid-crustal levels. This interpretation is supported by the range of magma compositions erupted over the lifetime of the current stratovolcanic edifice. Meanwhile, surrounding SEC have no large edifice slowing ascent, and are embedded in domains of extensional to transtensional stress regimes. As a result, our data suggest these mafic magmas ascend faster, and do not have time to evolve to higher-silica compositions, building minor mafic eruptive centres in areas of extension to transtension. Therefore, should periods of volcanic unrest be detected at Puyehue, timescales between unrest and potential eruption are likely to be longer than in the areas surrounding the stratovolcanic edifice where ascent may be more rapid.

By using carefully applied diffusion modelling to elucidate volcanic processes that would otherwise be masked by complex changing boundary conditions and mineral growth, we have revealed differences in mafic magma ascent within a small region of the CSVZ of Chile. In order to properly quantify the effect that the Puyehue edifice and varying upper crustal stress states have on mafic magma ascent, bespoke analogue or numerical models could be constructed to better link petrological inferences on magma ascent with geophysical observations of upper crustal stress state.

**Supplementary Information** The online version contains supplementary material available at <https://doi.org/10.1007/s00445-024-01740-w>.

**Acknowledgements** The authors wish to thank Eleonora Rivalta (GFZ, Università di Bologna) for valuable discussion, Bridie Davies for assistance in the field, Adrian Wood (BGS) for preparation of samples, Bertrand Lezé (UEA) and Graham Souch (Derby) for their technical expertise, and Lauren Martin and Maciej Farbicki (Derby) for assistance during data collection. Philipp Ruprecht, an anonymous reviewer,

and editor Julia Hammer are thanked for their constructive comments that led to improvements on this manuscript.

**Funding** This work was conducted as part of the ‘MagmaStress’ project funded by the Natural Environment Research Council (NERC): NE/S007520/1.

**Open Access** This article is licensed under a Creative Commons Attribution 4.0 International License, which permits use, sharing, adaptation, distribution and reproduction in any medium or format, as long as you give appropriate credit to the original author(s) and the source, provide a link to the Creative Commons licence, and indicate if changes were made. The images or other third party material in this article are included in the article’s Creative Commons licence, unless indicated otherwise in a credit line to the material. If material is not included in the article’s Creative Commons licence and your intended use is not permitted by statutory regulation or exceeds the permitted use, you will need to obtain permission directly from the copyright holder. To view a copy of this licence, visit <http://creativecommons.org/licenses/by/4.0/>.

## References

- Albert H, Costa F, Martí J (2015) Timing of magmatic processes and unrest associated with mafic historical monogenetic eruptions in Tenerife Island. *J Petrol* 56(10):1945–1966
- Alloway BV, Pearce NJG, Villarosa G, Outes V, Moreno PI (2015) Multiple melt bodies fed the AD 2011 eruption of Puyehue-Cordón Caulle. *Chile Scientific Reports* 5(1):1–8
- Angermann D, Klotz J, Reigber C (1999) Space-geodetic estimation of the Nazca-South America Euler vector. *Earth Planet Sci Lett* 171(3):329–334
- Basualto D, Tassara A, Lazo-Gil J, Franco-Marin L, Cardona C, San Martín J, Gil-Cruz F, Calabi-Floddy M, Farías C (2023) Anatomy of a high-silica eruption as observed by a local seismic network: the June 2011 Puyehue-Cordón Caulle event (southern Andes, Chile). *Solid Earth* 14(1):69–87
- Bell SK, Morgan DJ, Joy KH, Pernet-Fisher JF, Hartley ME (2023) Determining the thermal histories of Apollo 15 mare basalts using diffusion modelling in olivine. *Geochim Cosmochim Acta* 357:77–91
- Blundy J, Cashman K (2008) Petrologic reconstruction of magmatic system variables and processes. *Rev Mineral Geochem* 69(1):179–239
- Boschetti FO, Ferguson DJ, Cortés JA, Morgado E, Ebmeier SK, Morgan DJ, Romero JE, Silva Parejas C (2022) Insights into magma storage beneath a frequently erupting arc volcano (Villarrica, Chile) from unsupervised machine learning analysis of mineral compositions. *Geochem Geophys Geosyst* 23(4):2022GC010333
- Bucchi F, Lara LE, Gutiérrez F (2015) The Carrán-Los Venados volcanic field and its relationship with coeval and nearby polygenetic volcanism in an intra-arc setting. *J Volcanol Geoth Res* 308:70–81
- Caricchi L, Townsend M, Rivalta E, Namiki A (2021) The build-up and triggers of volcanic eruptions. *Nat Rev Earth Environ* 2(7):458–476
- Castro JM, Schipper CI, Mueller SP, Militzer AS, Amigo A, Parejas CS, Jacob D (2013) Storage and eruption of near-liquidus rhyolite magma at Cordón Caulle, Chile. *Bull Volcanol* 75:1–17
- Cembrano J, Lara L (2009) The link between volcanism and tectonics in the southern volcanic zone of the Chilean Andes: a review. *Tectonophysics* 471(1–2):96–113
- Cembrano J, Hervé F, Lavenu A (1996) The Liquiñe Ofqui fault zone: a long-lived intra-arc fault system in southern Chile. *Tectonophysics* 259(1–3):55–66
- Chamberlain KJ, Morgan DJ, Wilson CJ (2014) Timescales of mixing and mobilisation in the Bishop Tuff magma body: perspectives from diffusion chronometry. *Contrib Miner Petrol* 168:1–24
- Conway CE, Chamberlain KJ, Harigane Y, Morgan DJ, Wilson CJ (2020) Rapid assembly of high-Mg andesites and dacites by magma mixing at a continental arc stratovolcano. *Geology* 48(10):1033–1037
- Coombs ML, Wech AG, Haney MM, Lyons JJ, Schneider DJ, Schwaiger HF, Tepp G (2018) Short-term forecasting and detection of explosions during the 2016–2017 eruption of Bogoslof volcano Alaska. *Front Earth Sci* 6:122
- Costa F, Shea T, Ubide T (2020) Diffusion chronometry and the timescales of magmatic processes. *Nat Rev Earth Environ* 1(4):201–214
- Couperthwaite FK, Thordarson T, Morgan DJ, Harvey J, Wilson M (2020) Diffusion timescales of magmatic processes in the Moinui lava eruption at Mauna Loa, Hawaii, as inferred from bimodal olivine populations. *J Petrol* 61(7):egaa058
- Couperthwaite FK, Morgan DJ, Pankhurst MJ, Lee PD, Day JM (2021) Reducing epistemic and model uncertainty in ionic inter-diffusion chronology: a 3D observation and dynamic modeling approach using olivine from Piton de la Fournaise, La Réunion. *American Mineral J Earth Planetary Mater* 106(3):481–494
- Couperthwaite FK, Morgan DJ, Harvey J, Kahl M (2022) Pre-eruptive timescales from the historical Hapaimamo eruption at Mauna Loa, Hawaii ‘i. *J Volcanol Geoth Res* 432:107690
- Davis T, Bagnardi M, Lundgren P, Rivalta E (2021) Extreme curvature of shallow magma pathways controlled by competing stresses: insights from the 2018 Sierra Negra eruption. *Geophys Res Lett* 48(13):e2021GL093038
- DeSilva CM, Singer BS, Alloway BV, Moreno-Yaeger P (2023) Origin of the compositionally zoned Paso Puyehue Tephra, Antillanca Volcanic Complex, Chile. *J Volcanol Geoth Res* 444:107943
- Donaldson CH (1976) An experimental investigation of olivine morphology. *Contrib Miner Petrol* 57(2):187–213
- Faure F, Trolliard G, Nicollet C, Montel JM (2003) A developmental model of olivine morphology as a function of the cooling rate and the degree of undercooling. *Contrib Miner Petrol* 145(2):251–263
- Gerlach DC, Frey FA, Moreno-Roa H, Lopez-Escobar L (1988) Recent volcanism in the Puyehue—Cordon Caulle region, Southern Andes, Chile (40–5° S): petrogenesis of evolved lavas. *J Petrol* 29(2):333–382
- Gilbert DJ (2012) Pre-eruptive conditions at Lonquimay and Puyehue-Cordon Caulle volcanoes, Chile: framework for tectonic influences. <https://nbn-resolving.org/urn:nbn:de:gbv:8-diss-94325>
- Giuffrida M, Scandura M, Costa G, Zuccarello F, Sciotto M, Cannata A, Viccaro M (2021) Tracking the summit activity of Mt. Etna volcano between July 2019 and January 2020 by integrating petrological and geophysical data. *J. Volcanol Geotherm Res* 418:107350
- Global Volcanism Program (2021) Report on La Palma (Spain). In: Sennert SK (ed) Weekly volcanic activity report, 8–14 September 2021. Smithsonian Institution and US Geological Survey. [online]
- Gualda GA, Ghiorsio MS (2015) MELTS \_ Excel: a Microsoft Excel-based MELTS interface for research and teaching of magma properties and evolution. *Geochem Geophys Geosyst* 16(1):315–324
- Hickey RL, Frey FA, Gerlach DC, Lopez-Escobar L (1986) Multiple sources for basaltic arc rocks from the southern volcanic zone of the Andes (34–41 S): trace element and isotopic evidence for contributions from subducted oceanic crust, mantle, and continental crust. *J Geophys Res Solid Earth* 91(B6):5963–5983
- Hickey-Vargas R, Sun M, López-Escobar L, Moreno-Roa H, Reagan MK, Morris JD, Ryan JG (2002) Multiple subduction components in the mantle wedge: evidence from eruptive centers in the Central Southern volcanic zone Chile. *Geology* 30(3):199–202

- Hickey-Vargas R, Holbik S, Tormey D, Frey FA, Roa HM (2016a) Basaltic rocks from the Andean Southern Volcanic Zone: insights from the comparison of along-strike and small-scale geochemical variations and their sources. *Lithos* 258:115–132
- Hickey-Vargas R, Sun M, Holbik S (2016b) Geochemistry of basalts from small eruptive centers near Villarrica stratovolcano, Chile: evidence for lithospheric mantle components in continental arc magmas. *Geochim Cosmochim Acta* 185:358–382
- Holness MB, Anderson AT, Martin VM, MacLennan J, Passmore E, Schwindinger K (2007) Textures in partially solidified crystalline nodules: a window into the pore structure of slowly cooled mafic intrusions. *J Petrol* 48(7):1243–1264
- Jicha BR, Singer BS, Beard BL, Johnson CM, Moreno-Roa H, Naranjo JA (2007) Rapid magma ascent and generation of <sup>230</sup>Th excesses in the lower crust at Puyehue-Cordón Caulle, Southern Volcanic Zone Chile. *Earth Planet Sci Lett* 255(1–2):229–242
- Kahl M, Chakraborty S, Costa F, Pompilio M (2011) Dynamic plumbing system beneath volcanoes revealed by kinetic modeling, and the connection to monitoring data: an example from Mt. Etna. *Earth Planet Sci Lett* 308(1–2):11–22
- Kahl M, Mutch EJF, MacLennan J, Morgan DJ, Couperthwaite F, Bali E, Thordarson T, Guðfinnsson GH, Walshaw R, Buisman I, Buhre S, van der Meer QHA, Caracciolo A, Marshall EW, Rasmussen MB, Gallagher CR, Moreland WM, Höskuldsson Á, Askew RA (2022) Deep magma mobilization years before the 2021 CE Fagradalsfjall eruption Iceland. *Geology* 51(2):184–188
- Kahl M, Morgan DJ, Thornber C, Walshaw R, Lynn KJ, Trusdell FA (2023) Dynamics of magma mixing and magma mobilisation beneath Mauna Loa—insights from the 1950 AD Southwest Rift Zone eruption. *Bull Volcanol* 85(12):75
- Kavanagh JL, Burns AJ, Hazim SH, Wood EP, Martin SA, Hignett S, Dennis DJ (2018) Challenging dyke ascent models using novel laboratory experiments: implications for reinterpreting evidence of magma ascent and volcanism. *J Volcanol Geoth Res* 354:87–101
- Lara LE, Moreno H (2006) Geología del Complejo Volcánico Puyehue - Cordón Caulle, Región de Los Lagos. Servicio Nacional de Geología y Minería, Carta Geológica de Chile, Serie Geología Básica, No. 99, 1 mapa escala 1:50.000. Santiago
- Lara LE, Naranjo JA, Moreno H (2004) Rhyodacitic fissure eruption in Southern Andes (Cordón Caulle; 40.5 S) after the 1960 (Mw: 9.5) Chilean earthquake: a structural interpretation. *J Volcanol Geotherm Res* 138(1–2):127–138
- Lara LE, Lavenu A, Cembrano J, Rodríguez C (2006a) Structural controls of volcanism in transverse chains: resheared faults and neotectonics in the Cordón Caulle-Puyehue area (40.5 S), Southern Andes. *J Volcanol Geotherm Res* 158(1–2):70–86
- Lara LE, Moreno H, Naranjo JA, Matthews S, De Arce CP (2006b) Magmatic evolution of the Puyehue-Cordón Caulle Volcanic Complex (40 S), Southern Andean Volcanic Zone: from shield to unusual rhyolitic fissure volcanism. *J Volcanol Geoth Res* 157(4):343–366
- Lavenu A, Cembrano J (1999) Compressional-and transpressional-stress pattern for Pliocene and Quaternary brittle deformation in fore arc and intra-arc zones (Andes of Central and Southern Chile). *J Struct Geol* 21(12):1669–1691
- Le Maitre RW (1984) A proposal by the IUGS Subcommittee on the Systematics of Igneous Rocks for a chemical classification of volcanic rocks based on the total alkali silica (TAS) diagram: (on behalf of the IUGS Subcommittee on the Systematics of Igneous Rocks). *Aust J Earth Sci* 31(2):243–255
- Leeman WP, Smith DR (2018) The role of magma mixing, identification of mafic magma inputs, and structure of the underlying magmatic system at Mount St Helens. *Am Mineral* 103(12):1925–1944
- Longpré MA, Klügel A, Diehl A, Stix J (2014) Mixing in mantle magma reservoirs prior to and during the 2011–2012 eruption at El Hierro Canary Islands. *Geology* 42(4):315–318
- López-Escobar L, Parada MA, Hickey-Vargas R, Frey FA, Kempton PD, Moreno H (1995) Calbuco Volcano and minor eruptive centers distributed along the Liquiñe-Ofqui Fault Zone, Chile (41–42 S): contrasting origin of andesitic and basaltic magma in the Southern Volcanic Zone of the Andes. *Contrib Miner Petrol* 119(4):345–361
- Lubbers J, Kent AJ, de Silva S (2022) Thermal budgets of magma storage constrained by diffusion chronometry: the Cerro Galán ignimbrite. *J Petrol* 63(7):egac048
- Mangler MF, Petrone CM, Prytulak J (2022) Magma recharge patterns control eruption styles and magnitudes at Popocatepetl volcano (Mexico). *Geology* 50(3):366–370
- McGee LE, Brahm R, Rowe MC, Handley HK, Morgado E, Lara LE, Valdivia P (2017) A geochemical approach to distinguishing competing tectono-magmatic processes preserved in small eruptive centres. *Contrib Mineral Petrol* 172(6):1–26
- Morgado E, Parada MA, Contreras C, Castruccio A, Gutiérrez F, McGee LE (2015) Contrasting records from mantle to surface of Holocene lavas of two nearby arc volcanic complexes: Caburga-Huelemolle Small Eruptive Centers and Villarrica Volcano, Southern Chile. *J Volcanol Geoth Res* 306:1–16
- Morgado E, Parada MA, Morgan DJ, Gutiérrez F, Castruccio A, Contreras C (2017) Transient shallow reservoirs beneath small eruptive centres: Constraints from Mg-Fe interdiffusion in olivine. *J Volcanol Geoth Res* 347:327–336
- Morgado E, Morgan DJ, Castruccio A, Ebmeier SK, Parada MÁ, Brahm R, Walshaw R (2019) Old magma and a new, intrusive trigger: using diffusion chronometry to understand the rapid-onset Calbuco eruption, April 2015 (Southern Chile). *Contrib Mineral Petrol* 174(7):1–11
- Mutch EJ, MacLennan J, Holland TJ, Buisman I (2019a) Millennial storage of near-Moho magma. *Science* 365(6450):260–264
- Mutch EJ, MacLennan J, Shorttle O, Edmonds M, Rudge JF (2019b) Rapid transcristal magma movement under Iceland. *Nat Geosci* 12(7):569–574
- Namur O, Montalbano S, Bolle O, Vander Auwera J (2020) Petrology of the April 2015 eruption of Calbuco volcano, southern Chile. *J Petrol* 61(8):egaa084
- Naranjo JA, Singer BS, Jicha BR, Moreno H, Lara LE (2017) Holocene tephra succession of Puyehue-Cordón Caulle and Antilanca/Casablanca volcanic complexes, southern Andes (40–41 S). *J Volcanol Geoth Res* 332:109–128
- Neave DA, Putirka KD (2017) A new clinopyroxene-liquid barometer, and implications for magma storage pressures under Icelandic rift zones. *Am Miner* 102(4):777–794
- Neave DA, Passmore E, MacLennan J, Fitton G, Thordarson T (2013) Crystal–melt relationships and the record of deep mixing and crystallization in the ad 1783 Laki Eruption Iceland. *J Petrol* 54(8):1661–1690
- Oeser M, Ruprecht P, Weyer S (2018) Combined Fe-Mg chemical and isotopic zoning in olivine constraining magma mixing-to-eruption timescales for the continental arc volcano Irazú (Costa Rica) and Cr diffusion in olivine. *Am Miner* 103(4):582–599
- Oyarzún A, Lara LE, Tassara A (2022) Decoding the plumbing system of Nevados de Chillán Volcanic complex, Southern Andes. *J Volcanol Geoth Res* 422:107455
- Pérez-Estay N, Ruz-Ginouves J, Pérez-Flores P, Sielfeld G, Roquer T, Cembrano J (2023) Decoding the state of stress and fluid pathways along the Andean Southern Volcanic Zone. *Commun Earth Environ* 4(1):390
- Pinel, V., & Jaupart, C. (2000). The effect of edifice load on magma ascent beneath a volcano. *Philosophical Transactions of the*

- Royal Society of London. Series A: Mathematical, Physical and Engineering Sciences, 358(1770), 1515–1532
- Pioli L, Scalisi L, Costantini L, Di Muro A, Bonadonna C, Clavero J (2015) Explosive style, magma degassing and evolution in the Chaimilla eruption, Villarrica volcano, Southern Andes. *Bull Volcanol* 77:1–14
- Putirka KD (2008) Thermometers and barometers for volcanic systems. *Rev Mineral Geochem* 69(1):61–120
- Putirka KD, Perfit M, Ryerson FJ, Jackson MG (2007) Ambient and excess mantle temperatures, olivine thermometry, and active vs passive upwelling. *Chem Geol* 241(3–4):177–206
- Rivalta E, Böttlinger M, Dahm T (2005) Buoyancy-driven fracture ascent: Experiments in layered gelatine. *J Volcanol Geoth Res* 144(1–4):273–285
- Rivalta E, Taisne B, Bungler AP, Katz RF (2015) A review of mechanical models of dike propagation: schools of thought, results and future directions. *Tectonophysics* 638:1–42
- Rivalta E, Corbi F, Passarelli L, Acocella V, Davis T, Di Vito MA (2019) Stress inversions to forecast magma pathways and eruptive vent location. *Sci Adv* 5(7):eaau9784
- Roman A, Jaupart C (2014) The impact of a volcanic edifice on intrusive and eruptive activity. *Earth Planet Sci Lett* 408:1–8
- Rosenau M, Melnick D, Echtler H (2006) Kinematic constraints on intra-arc shear and strain partitioning in the southern Andes between 38 S and 42 S latitude. *Tectonics*, 25(4). <https://doi.org/10.1029/2005TC001943>
- Ruth DC, Costa F, Bouvet de Maisonneuve C, Franco L, Cortés JA, Calder ES (2018) Crystal and melt inclusion timescales reveal the evolution of magma migration before eruption. *Nat Commun* 9(1):2657
- Salas PA, Rabbia OM, Hernández LB, Ruprecht P (2017) Mafic monogenetic vents at the Descabezado Grande volcanic field (35.5 S–70.8 W): the northernmost evidence of regional primitive volcanism in the Southern Volcanic Zone of Chile. *Int J Earth Sci* 106:1107–1121
- Salas P, Ruprecht P, Hernández L, Rabbia O (2021) Out-of-sequence skeletal growth causing oscillatory zoning in arc olivines. *Nat Commun* 12(1):4069
- Schipper CI, Castro JM, Tuffen H, James MR, How P (2013) Shallow vent architecture during hybrid explosive–effusive activity at Cordón Caulle (Chile, 2011–12): evidence from direct observations and pyroclast textures. *J Volcanol Geoth Res* 262:25–37
- Sepúlveda F, Lahsen A, Bonvalot S, Cembrano J, Alvarado A, Letelier P (2005) Morpho-structural evolution of the Cordón Caulle geothermal region, Southern Volcanic Zone, Chile: insights from gravity and  $^{40}\text{Ar}/^{39}\text{Ar}$  dating. *J Volcanol Geoth Res* 148:165–189
- Shejwalkar A, Coogan LA (2013) Experimental calibration of the roles of temperature and composition in the Ca-in-olivine geothermometer at 0.1 MPa. *Lithos* 177:54–60
- Singer BS, Jicha BR, Harper MA, Naranjo JA, Lara LE, Moreno-Roa H (2008) Eruptive history, geochronology, and magmatic evolution of the Puyehue-Cordón Caulle volcanic complex Chile. *Geol Soc Am Bull* 120(5–6):599–618
- Sparks RSJ (2003) Forecasting volcanic eruptions. *Earth Planet Sci Lett* 210(1–2):1–15
- Sun SS, McDonough WF (1989) Chemical and isotopic systematics of oceanic basalts: implications for mantle composition and processes. *Geol Soc Lond Spec Publ* 42(1):313–345
- Tassara A, Echaurren A (2012) Anatomy of the Andean subduction zone: three-dimensional density model upgraded and compared against global-scale models. *Geophys J Int* 189(1):161–168
- Vander Auwera J, Montalbano S, Namur O, Bechon T, Schiano P, Devidal JL, Bolle O (2021) The petrology of a hazardous volcano: Calbuco (Central Southern Volcanic Zone, Chile). *Contrib Miner Petrol* 176:1–34
- Watanabe T, Koyaguchi T, Seno T (1999) Tectonic stress controls on ascent and emplacement of magmas. *J Volcanol Geoth Res* 91(1):65–78
- Wehrmann H, Hoernle K, Jacques G, Garbe-Schönberg D, Schumann K, Mahlke J, Lara LE (2014) Volatile (sulphur and chlorine), major, and trace element geochemistry of mafic to intermediate tephra from the Chilean Southern Volcanic Zone (33–43 S). *Int J Earth Sci* 103:1945–1962
- Weis D, Kieffer B, Maerschalk C, Barling J, De Jong J, Williams GA, Hanano D, Pretorius W, Mattielli N, Scoates JS, Goolaerts A (2006) High-precision isotopic characterization of USGS reference materials by TIMS and MC-ICP-MS. *Geochem Geophys Geosyst* 7(8)
- Wilson CJ, Cooper GF, Chamberlain KJ, Barker SJ, Myers ML, Illsley-Kemp F, Farrell J (2021) No single model for supersized eruptions and their magma bodies. *Nat Rev Earth Environ* 2(9):610–627
- Winslow H, Ruprecht P, Stelten M, Amigo A (2020) Evidence for primitive magma storage and eruption following prolonged equilibration in thickened crust. *Bull Volcanol* 82(11):69
- Winslow H, Ruprecht P, Gonnermann HM, Phelps PR, Muñoz-Saez C, Delgado F, Pritchard M, Amigo A (2022) Insights for crystal mush storage utilizing mafic enclaves from the 2011–12 Cordón Caulle eruption. *Sci Rep* 12(1):9734
- Zellmer GF, Freymuth H, Cembrano JM, Clavero JE, Veloso EA, Sielfeld GG (2014) Altered mineral uptake into fresh arc magmas: insights from U-Th isotopes of samples from Andean volcanoes under differential crustal stress regimes. *Geol Soc Lond Spec Publ* 385(1):185–208